Source localization using rational approximation on plane sections

Maureen Clerc, Juliette Leblond, Jean-Paul Marmorat, Théodore
Papadopoulo

▶ **To cite this version:**

INRIA

Source localization using rational approximation on plane sections

M. Clerc, J. Leblond, J.-P. Marmorat, T. Papadopoulo

N° 7704

Août 2011

Domaines 1,5

Rapport de recherche

Source localization using rational approximation on plane sections

M. Clerc, J. Leblond, J.-P. Marmorat, T. Papadopoulo

Domaines : Mathématiques appliquées, calcul et simulation
STIC pour les sciences de la vie et de l'environnement
Équipes-Projets INRIA Athena, Apics, et CMA, Ecole des Mines

Abstract: In functional neuroimaging, a crucial problem is to localize active sources within the brain non-invasively, from the knowledge of the electromagnetic measurements outside the head. Identification of point sources from boundary measurements is an ill-posed inverse problem. In the case of electroencephalography (EEG), measurements are only available at electrode positions, the number of sources is not known in advance, and the medium within the head is inhomogeneous. This paper presents a new method for EEG source localization, based on rational approximation techniques in the complex plane. The method is used in the context of a nested sphere head model, in combination with a cortical mapping procedure. Results on simulated data prove the applicability of the method in the context of realistic measurements configurations.

Key-words: inverse EEG problem, cortical mapping, source localization, rational approximation

Localisation de sources par approximation rationnelle sur des sections planes

Résumé : Un problème crucial en imagerie cérébrale (fonctionnelle ou clinique) consiste en la localisation (par des techniques non invasives) de sources de l'activité cérébrale dans le cerveau, depuis des mesures éléctromagnétiques prélevées à la surface ou à l'extèrieur de la tête. L'identification de sources ponctuelles depuis des mesures frontière constitue un problème inverse mal posé. Concernant l'électroencéphalographie (EEG), les mesures sont disponibles aux positions des électrodes, le nombre de sources n'est pas connu à l'avance, et le milieu conducteur à l'intérieur de la tête est inhomogène. Ce travail présente une nouvelle méthode de localisation de sources en EEG, basée sur des techniques d'approximation rationnelle dans le plan complexe. Cette méthode est développée pour un modèle sphérique de tête, à plusieurs couches de conductivité constante (scalp, crâne, cerveau), en combinaison avec une procédure de transmission des données, depuis le scalp jusqu'à la surface du cerveau. Des résultats numériques depuis des données simulées dans des configurations réalistes démontrent l'applicabilité de la méthode.

Mots-clés : problème inverse en Électroencéphalographie, localisation de sources, approximation rationnelle

1 Introduction

Electromagnetic Source Mapping aims at localizing active sources within the brain from measurements of the electromagnetic field they produce, which can be measured passively outside the head. This article deals more specifically with the electric potential which is measured using Electroencephalography (EEG).
Estimating neural current sources located within the bra1in from outside measurements falls into a category of inverse source problems, that are severely ill-posed in general, mainly due to the lack of continuity and stability, but also to non-uniqueness [Isakov, 1998, Vessella, 1992].
When a limited number of sources are modeled as pointwise and dipolar, there are in general more measurements than unknowns, and it has been proved that the inverse problem of source estimation has a unique solution [Badia and Ha-Duong, 2000]. However, even in this pointwise and dipolar case, solutions to the inverse source problem are often unstable, in particular with respect to the number of sources.
Several families of methods exist to solve the inverse source localization problem, when sources can be modeled as the superposition of a small number of dipoles [Scherg et al., 1999]. *Dipole Fitting* methods must minimise a non-convex goal function, yielding an outcome that is unstable with respect to the number of dipoles in the model [Cuffin, 1995]. Whenever this number is assumed to be known a priori, an algebraic (scanning) method has been proposed in [Badia and Ha-Duong, 2000], which requires rank computation of related matrices. In practise, one does not know this number in advance, and learning this model order is far from trivial [Bénar et al., 2005]. If the sources are decorrelated in time, analyzing the covariance matrix of the measured data provides an estimate of the number of active dipoles. The number of sources is indeed equal to the number of singular values that are significantly different from zero. The *MUSIC Method* first applies a principal component analysis (PCA) to the measurements, identifies a "signal subspace" of which the analysis subsequently determines the dipole positions [Mosher et al., 1992]. In practise, the dimensionality of the signal subspace is difficult to determine, and the dipoles are extracted one at a time by seeking the global maximum of a contrast function among all possible source positions. *MUSIC* can thus only be applied if the sources are well modeled by a small number of asynchronous dipoles. With the stronger assumption of decorrelated sources, another method, *Beamforming*, can also estimate active sources, by scanning a region of interest, and by comparing the covariance of the measurement to that of the baseline, measured in time windows that do not contain the activity of interest [Van Veen and Buckley, 1988].
This article proposes a new approach, which, as *MUSIC* and *Beamforming*, requires no prior information on the number of sources. However, unlike *MUSIC* or *Beamforming*, which require as input consecutive measurements within a time window, the proposed method works instant by instant, and *a fortiori*, does not require sources to be decorrelated across time.
Our method belongs to a new category of source estimation algorithms that are grounded in Harmonic Analysis and Best Approximation theory, and offer stability [Baratchart et al., 2006, Kandaswamy et al., 2009]. These analytical methods directly localize the sources as the singularities of the potential from boundary measurements.

The type of geometry and of boundary data which they require do not necessarily coincide with actual measurements. Indeed, these methods usually work in a homogeneous domain, and an explicit parametrization may be needed for its boundary.

We present our constructive approach to this inverse problem, in the framework of a (classical) spherical geometry. Under quasi-static assumptions, Maxwell's equations lead to a formulation of the electric potential u as a solution to Laplace's equation. In the innermost layer (the brain), there may be singularities due to the presence of current sources. These singularities are to be localized from available data on the outer boundary (the scalp). The core of our inverse solution relies on approximation schemes that are meant to operate inside homogeneous domains, and not in such a nested geometry. Hence, a preliminary stage consists of mapping to the cortex the data initially measured on the surface of the scalp. This *Cortical Mapping* problem is a Cauchy (transmission) problem for the Laplace operator [Clerc and Kybic, 2007].

Source detection from cortical data is another classical inverse problem for the Laplace operator, that consists of recovering an unknown number of pointwise sources within a homogeneous domain from measurements of the potential and its normal derivative on the boundary.

When the domain is a spherical ball, then the above issue is equivalent to a sequence of 2D inverse problems, each of which consists of recovering the singularities of some function f in a disk from the knowledge of f on the boundary circle [Baratchart et al., 2006]. Consequently, we apply to these 2D problems a technique inspired by that described in [Baratchart et al., 2005] that relies on approximating f on the boundary circle by a rational function with poles in the disk.

Finally, we locate the singularities by analyzing the cluster of these poles. Geometrical restriction to spherical domains allows one to make explicit (and not too complex, in a preliminary feasibility study) the behaviour of the 2D singularities with respect to the 3D sources, which is granted by our recovery scheme. The outline is as follows: Section 2 introduces the inverse problem, and Section 3 presents the solution proposed in this paper. Section 4 demonstrates the method on numerical examples. The paper also includes a conclusion in Section 5 and technical Appendices that detail some mathematical aspects of the method.

2   The inverse problem

2.1   Model setting

In a simplified spherical model, the head is assumed to be the union of three disjoint homogeneous spherical layers[1] Ω_0, Ω_1, Ω_2, namely the brain, the skull, and the scalp, within a non-conductive medium Ω_3 representing the air. Up to a rescaling, one may assume the ball Ω_0 representing the brain to have radius 1 and to be centered at the origin. The spheres separating the volumes Ω_i are denoted $\mathbb{S}_0$, $\mathbb{S}_1$ and $\mathbb{S}_2$ (see Figure 1). The conductivity in each Ω_i is denoted σ_i. For simplicity and without loss of generality, we assume that $\sigma_0 = 1$. Then, we define a piecewise constant function σ in $\mathbb{R}^3$ by $\sigma_{|\Omega_i} = \sigma_i$. The current

---

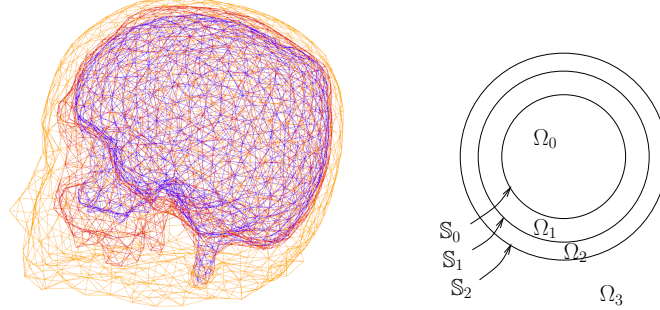[1]In the remainder of this article, all domains are supposed to be open.

Figure 1: A nested conductor model for the head (left), in which brain, skull and scalp have a homogeneous conductivity. Our 3D spherical nested model (right, 2D view), where the brain and scalp (Ω_0, Ω_2) conductivity is 0.33, the skull conductivity is 0.0042 and the air Ω_3 is non-conductive.

sources are modeled as dipoles situated strictly inside the inner layer Ω_0 and are characterised by their number n, their positions $C_k \in \Omega_0$ and their moments $p_k \in \mathbb{R}^3$, $k = 1, ..., n$.

2.2 The inverse problem

The potential created by the dipolar sources (C_k, p_k) located inside Ω_0 is a solution to the forward problem

$$(\text{FP}) \quad \begin{cases} \nabla \cdot (\sigma \nabla u) = \mathcal{S} = \sum_{k=1}^{n} p_k \, . \, \nabla \, \delta_{C_k} \text{ in } \mathbb{R}^3 \\ \sigma \partial_\nu u_{|_{\mathbb{S}_2}} = 0 \text{ (current flux)} \end{cases} \quad (1)$$

where ν denotes the outward unit normal vector to the surfaces. The homogeneous Neumann boundary condition is due to the fact that the outer medium (air) is non-conductive. The current flowing through the neck is neglected.

Let K denote a set of points on $\mathbb{S}_2$, representing electrode positions. The inverse source localization problem (IP) associated to the forward problem (FP) is then the following:

(IP) *Given measurements of u on K, find the number of unknown pointwise dipolar sources, their positions $C_k \in \Omega_0$ and their moments $p_k \in \mathbb{R}^3$, such that u satisfies (FP).*

2.3 Properties of solutions to (IP)

Mathematical properties of (IP) have been established when the data is known in an open subset K of the boundary. In our case, the data is only known on a discrete set, but it is assumed that the underlying potential is smooth enough so that it is well approximated on an open set K from the data. Uniqueness of solutions to (IP) (identifiability from boundary measurements) has been established in [Badia and Ha-Duong, 2000]. If two finite distributions of pointwise dipolar sources generate the same potential on some open subset K of $\mathbb{S}_2$, then they are identical.

Stability properties for (IP) may only hold for smooth enough boundary data on K (in Sobolev spaces). This is due to the classical ill-posedness of Cauchy-type issues (Section 3.1.1) [Alessandrini et al., 2009, Isakov, 1998, Phung, 2003, Zghal, 2010]. Concerning the source problem in homogeneous domain (sections 3.3 and 3.4), stability results are established in [Badia, 2005, Vessella, 1992].

3 Solution to the inverse problem (IP)

The resolution of the above inverse problem (IP) consists of two main steps as represented in the flowchart in Figure 2.
Data Transmission from $\mathbb{S}_2$ to $\mathbb{S}_0$, which involves:

- **Cortical Mapping** (Section 3.1.1): the data is transmitted from the surface of the scalp $\mathbb{S}_2$ where it is measured (on electrodes) onto the surface $\mathbb{S}_0$ of the brain.

- **Harmonic Projection** (Section 3.1.2): filtering out possible outer sources by keeping only the information related to the effective inner sources in Ω_0.

Source Recovery in Ω_0 from data on $\mathbb{S}_0$, which involves:

- **Plane Sections** (Section 3.2): the sphere $\mathbb{S}_0$ is sliced along families of parallel planes, perpendicular to a chosen axis, yielding disks inside which the singularities will be sought.

- **Planar Singularity Detection** (Section 3.3): 2D approximation techniques are used to find the planar singularities on the plane sections of Ω_0 (disks).

- **3D Source Localization** (Section 3.4): for a putative number of sources, the sources are localized in 3D by analyzing the sets of planar singularities.

The Data Transmission step uses the approach proposed in [Clerc and Kybic, 2007] while the Source Recovery step uses the one described in [Baratchart et al., 2006] (see also [Abda et al., 2009], in two dimensions).

3.1 Data Transmission

3.1.1 Cortical Mapping

The goal, as recalled in Figure 2, is to estimate the values of the potential and the normal current on the cortex, from the values on electrodes of a potential that satisfies the Forward Problem (1). This Forward Problem can be decomposed in each of the three layers Ω_i, $i = 0, 1, 2$. By assumption, there are no sources outside the inner volume Ω_0, hence the potential u satisfies a homogeneous Laplace equation in the layers Ω_1 and Ω_2:

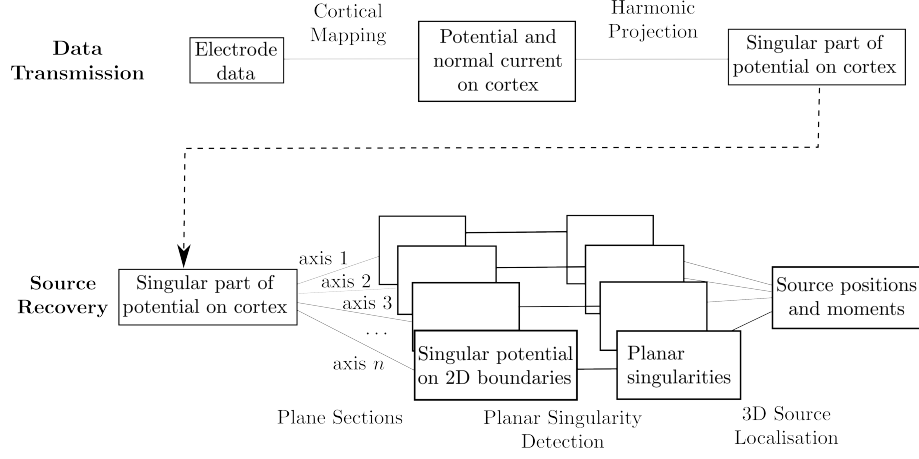$$\Delta u = 0 \text{ in } \Omega_i, i = 1, 2.$$

Figure 2: Flowchart of the Source Localization method, consisting of two main steps: Data Transmission and Source Recovery. Source Recovery makes use of a 2D Rational Approximation technique, which is run independently on slices of the domain. The Planar Singularities are then analyzed jointly to yield the positions and moments of the sources.

The continuity of the potential and of the normal current across the interfaces are expressed through the following transmission conditions:

$$u^+ = u^- \text{ on } \mathbb{S}_i, \ i = 0, 1, \tag{2}$$

$$\text{and } \sigma_{i+1} \partial_\nu u^+ = \sigma_i \partial_\nu u^- \text{ on } \mathbb{S}_i, \ i = 0, 1, \tag{3}$$

where superscripts $+$ and $-$ indicate the limiting values when approaching $\mathbb{S}_i$ from Ω_{i+1} (outside) and Ω_i (inside), respectively.

The Data Transmission problem which we aim to solve is a Cauchy Problem (CP), for u harmonic within Ω_1 and Ω_2, satisfying the transmission conditions (2-3):

(CP) *Given measurements u_K of u on $K \subset \mathbb{S}_2$ and given that $\partial_\nu u = 0$ on $\mathbb{S}_2$, find the values $g = u_{|\mathbb{S}_0}$ and $\phi = \partial_\nu u_{|\mathbb{S}_0}^-$ on $\mathbb{S}_0$.*

Solving (CP) is non-trivial, because the Cauchy problem for the Laplace equation is the prototype of an ill-posed problem. Indeed, (CP) has similar stability properties to those described in Section 2.3 for $K \subset \mathbb{S}_0$. Regularization schemes have been proposed in [Atfeh et al., 2010, Kozlov et al., 1992]. We solve the Cortical Mapping with a regularized Tikhonov method deriving from a "boundary elements" formulation of the problem (this step is thus not limited to spherical interfaces): from its values u_K on the measurement set K, u is estimated, along with $\sigma \partial_\nu u$, on the three surfaces $\mathbb{S}_2$, $\mathbb{S}_1$, and $\mathbb{S}_0$. This method, originally presented in [Clerc and Kybic, 2007], is detailed in A.

3.1.2 Harmonic Projection (in $\mathbb{R}^3$)

After the Cortical Mapping step has provided the potential $g = u$ and its normal derivative $\phi = \partial_\nu u$ on the surface of the cortex $\mathbb{S}_0$, the potential u satisfies in

Ω_0 an equation of the form:

$$
\begin{cases}
\Delta\,u = \mathcal{S} = \displaystyle\sum_{k=1}^{n} p_k\,.\,\nabla\,\delta_{C_k} \ \text{in}\ \Omega_0\,, \\[2mm]
\partial_\nu u \,=\, \phi\,,\quad u\,=\,g\ \text{on}\ \mathbb{S}_0\,.
\end{cases}
\tag{4}
$$

From g and ϕ on $\mathbb{S}_0$, we first look for the part u_a of the potential u which is harmonic outside the ball Ω_0, vanishes at ∞, and still contains on $\mathbb{S}_0$ all the information on the distribution of sources.

Knowing that the potential u in Ω_0 is solution of (4), let u_a be the convolution of $\mathcal{S}$ with the Green function for the Laplacian in $\mathbb{R}^3$:

$$
u_a(x) = \sum_{k=1}^{n} \frac{\langle p_k,\ x - C_k\rangle}{4\pi\,|x - C_k|^3}\,,\ x \neq C_k\,,
\tag{5}
$$

where the brackets $\langle\,,\,\rangle$ denote the scalar product in $\mathbb{R}^3 \times \mathbb{R}^3$. Note that:

$$
\Delta\,u_a = \Delta\,u = \mathcal{S}\ \text{in}\ \Omega_0\,,
$$

$$
\text{while}\ \Delta\,u_a = 0\ \text{in}\ \mathbb{R}^3 \setminus \Omega_0,\ \text{and}\ \lim_{|x|\to\infty} |u_a(x)| = 0\,.
$$

Consequently, for $x \in \Omega_0 \setminus \{C_k\}$, we have:

$$
u(x) = h(x) + u_a(x) = h(x) + \sum_{k=1}^{n} \frac{\langle p_k,\ x - C_k\rangle}{4\pi\,|x - C_k|^3}\,,
$$

for a harmonic function h in Ω_0.

In practise, u_a is computed from the available boundary data g and ϕ on $\mathbb{S}_0$ by expanding u there on the basis of spherical harmonics [Baratchart et al., 2006, Dautray and Lions, 2000]. Indeed, u being a harmonic function in a neighbourhood of $\mathbb{S}_0$, the coefficients of its expansion on $\mathbb{S}_0$ of negative indices coincide with those of u_a. They are given through a linear system, by identification with the coefficients of the spherical harmonics expansions of the discretized g and ϕ on $\mathbb{S}_0$.

Figure 3 shows the singular part u_a of the potential, computed from its expression (5) on $\mathbb{S}_0$, from $n = 2$ sources $C_1 = (0.5, 0.5, 0.5)$, $C_2 = (0.5, -0.5, -0.4)$ with moments $p_1 = (1, 1, 1)$, $p_2 = (-1, 1, 1)$.

3.2   From 3D to 2D

Given u_a, we can now formulate an *inverse source recovery problem* in Ω_0:

(SP) *Given u_a on $\mathbb{S}_0$, find the number of unknown pointwise dipolar sources, their locations $C_k \in \Omega_0$ and their moments $p_k \in \mathbb{R}^3$, such that u_a satisfies (5).*

Following [Baratchart et al., 2006], we first study the singularities of u_a^2 on plane sections of Ω_0, where the function can be analytically extended to the complex plane.

The ball Ω_0 is sliced along a family of P planes, Π_p, $p = 1, \cdots, P$, parallel to some plane $\Pi \subset \mathbb{R}^3$. The intersections of the planes Π_p with Ω_0 are disks D_p, whose boundaries are circles T_p (intersections $\Pi_p \cap \mathbb{S}_0$). The Data Transmission
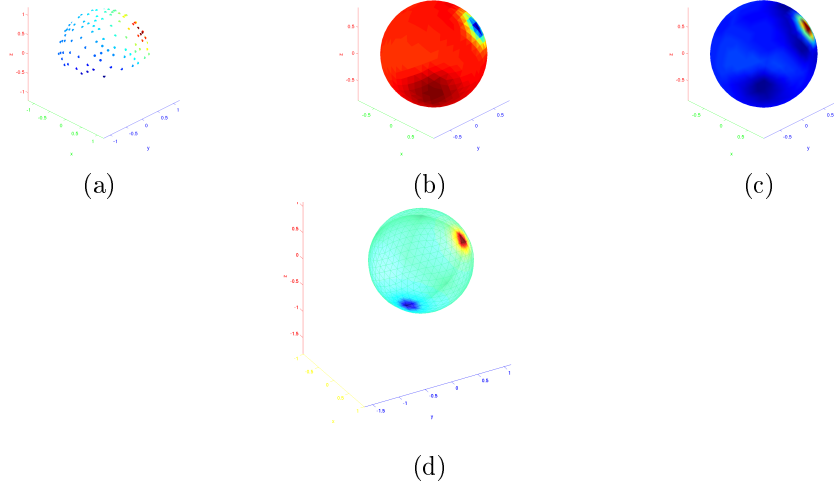
(a) (b) (c)

(d)

Figure 3: Data Transmission. Cortical Mapping: from electrode data (a), yielding the normal current (b) and the potential (c) on the cortical surface. Harmonic Projection: (d) representation on the cortex $\mathbb{S}_0$ of the singular part u_a of the potential, whose singularities are restricted to Ω_0.
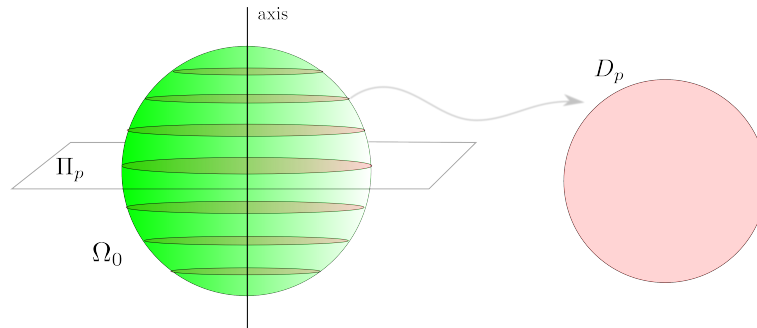

Figure 4: Plane Sections. Ω_0 is sliced into disks D_p by a series of parallel planes Π_p.

step (Section 3.1) has provided the singular part u_a of the potential on $\mathbb{S}_0$, and we now consider its restriction to each circle T_p.

The computations that follow are detailed in B. Denote by (x_1, x_2, x_3) the Cartesian coordinates in $\mathbb{R}^3$. Choose for simplicity $\Pi = \{x_3 = 0\}$ (this is always possible by composition with a rotation) whence $\Pi_p = \{x_3 = x_{3,p}\}$. For some fixed $x_{3,p} \in (-1, 1)$, let

$$x \in T_p: \ x = (x_1, x_2, x_{3,p}), \ r_p = \sqrt{1 - x_{3,p}^2}, \ z = (x_1 + i\,x_2)/r_p, \qquad (6)$$

where r_p is the radius of the circle T_p, and $z \in T$ is the normalised complex affix associated to $x \in T_p$.

From u_a on T_p, we build the *complex variable* function f_p on the unit circle $T \subset \mathbb{C}$ (the complex plane) as follows.

$$f_p(z) = u_a^2(x_1, x_2, x_{3,p}), \tag{7}$$

For fixed p, the function f_p coincides with the trace on T of a function defined on $\mathbb{C}$ except at singularities: due to the n sources C_k, this extended function (that we still call f_p) has n singularities inside the unit disk D (as well as n related singularities outside the closed disk $\overline{D}$).

Indeed, let us denote the source coordinates by $C_k = (x_{1,k}, x_{2,k}, x_{3,k})$, and their corresponding complex affix by $z_k = x_{1,k} + ix_{2,k}$, for $k = 1, \ldots, n$. Assuming $z_k \neq 0^2$, we have from (5), (7), at $x \in T_p$ and corresponding complex affix $z \in T$ through (6):

$$f_p(z) = \left[\sum_{k=1}^{n} \frac{\varphi_{k,p}(z)}{(z - s_{k,p})^{3/2}} \right]^2 \tag{8}$$

where $s_{k,p}$ are the singularities induced inside D by the source C_k and $\varphi_{k,p}$ are smooth functions in $\overline{D}$.

The localization of $s_{k,p}$ then leads to that of C_k. Indeed, the complex argument of $s_{k,p}$ is independent of p, and equal to the argument of z_k, which allows us to determine the number n of sources. Further, for fixed k, when p varies, the quantity $r_p |s_{k,p}|$ attains its maximal value, equal to $|z_k|$, when $x_{3,k} = x_{3,p}$, in the slice p corresponding to C_k.

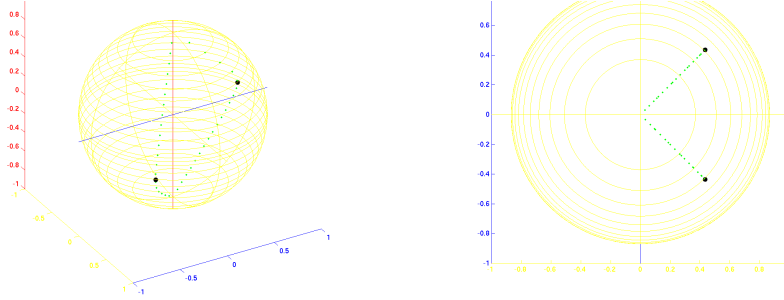Figure 5 shows the trajectories of the singularities $s_{k,p}$ in a two sources case.

Figure 5: True sources C_1, C_2 and theoretical singularities $s_{1,p}, s_{2,p}$, $p = 1, \cdots, P$, which when joining the dots form singular lines l_k (see Section 3.4: 3D view (left), top view (right).

3.3 Recovering 2D singularities

This section deals with the computation of the singularities $s_{k,p}$ from the sliced boundary data f_p on T, given by (7) at fixed p.

From formula (8), it can be seen that the function f_p has the following properties:

---

[2]This is generically true with respect to the plane Π. See however B for the degenerated situation where $z_k = 0$.

- If there is a single source ($n = 1$), then f_p is exactly a rational function with a single triple pole in D at position $s_{1,p}$:

$$f_p(z) = \frac{\varphi_{1,p}^2(z)}{(z - s_{1,p})^3} \, .$$

$$(9)$$

- If there are multiple singularities ($n \geq 2$), f_p is no longer a rational function (because of terms with power $3/2$ at the denominator of (8)). In this situation, the $s_{k,p}$ are both (triple) *poles* and *branchpoints* (of order $3/2$)[3]. Yet, f_p can be well approximated on the boundary T by a rational function with poles in D, see C and [Baratchart et al., 2006], [Baratchart and Yattselev, 2009].

This gives rise to the following algorithm that provides estimates $\widehat{s_{k,p}}$ of $s_{k,p}$ from sample values $\widehat{f}_p$ built from (7).

Finding Planar Singularities $\widehat{s_{k,p}} \simeq s_{k,p}$ from Cortical Data $\widehat{f}_p$

1. Choose the number n of sources.

2. Find initial values $s_{k,p}^*$ of $s_{k,p}$, to be the poles of a rational approximation f_p^* of f_p with appropriate degree (depending on n).

3. If $n = 1$ then $\widehat{s_{k,p}} = s_{k,p}^*$.

4. Otherwise, for f_p linked to $s_{k,p}$ by (8) and starting with the initial values $s_{k,p}^*$, find $\widehat{s_{k,p}}$ by minimizing (gradient descent) the criterion:

$$\widehat{s_{k,p}} = \arg\min_{s_{k,p}} \left\| \widehat{f}_p - f_p \right\| \, .$$

Remark 1 Though it should become an output of the proposed method, the number n is a necessary preliminary guess in the present algorithm.
In point (iv), $\| \, \|$ is the l^2 norm on T. The data f_p is assumed to be given either by a number of its pointwise values on T, or by a number of its Fourier coefficients, using the spherical harmonics expansion of u_a on $\mathbb{S}_0$ from Section 3.1.2. From this Fourier expansion, we shall keep only the part with negative indices, for it is enough to account for the singularities of f_p in D (see C.2), that we still call f_p, for simplicity.

Strategies for achieving step (ii) of this algorithm are discussed in C.
The present Planar Singularity Detection step must be performed with several slicing directions Π, in order to get more accuracy on the localization process and to separate sources (see Section 3.4 and [Marmorat et al., 2002, Marmorat and Olivi, 2004]).

---

[3] Recall that a pole (or polar singularity) is the zero of some polynomial at the denominator of the function, while a branchpoint is the singular point of some multivalued complex analytic function, as log or square-root.

3.4 From estimated singularities to sources positions and moments

Given a slicing direction Π, the method described in Section 3.3 provides estimates of the singularities $\widehat{s_{k,p}}$ of f_p in each slice. But, we know from Section 3.2 that the points $(r_p s_{k,p})_{k,p}$ are organized along as many lines l_k as there are sources ($k = 1 \ldots n$, see the lines formed by green dots in Figure 5).

3.4.1 Sources from a single slicing direction

Each line l_k is (generically, for most slicing directions) associated with one of the sources C_k and has the following theoretical properties (from section 3.2):

1. l_k lies in a single half-plane H_k defined by C_k and by the direction of the slicing plane Π: H_k contains C_k and is orthogonal to Π;

2. l_k goes through its associated source C_k. At this point, the radial distance of the line l_k to the boundary of H_k (the diameter of $\mathbb{S}_0$ orthogonal to Π) reaches its maximum.

The first property is used to group the points $r_p\widehat{s_{k,p}}$ into n estimated lines $\widehat{l_k}$. To do so, these points are clustered in n classes by applying Matlab's algorithm `clusterdata` to their polar angles. For each class, the best fitting half-plane $\widehat{H_k}$ is then estimated using a least-squares algorithm and the points are reprojected on that plane, providing us with an estimation $\widehat{l_k}$ of the line l_k. The polar angle of $\widehat{H_k}$ is an approximation of the complex argument $\operatorname{Arg}\widehat{z_k}$ of $\operatorname{Arg} z_k$. We can now compute $|z_k|$ using the second above property as:

$$\widehat{|z_k|} = \max_{p \in 1,\ldots,P}\{|r_p\widehat{s_{k,p}}| \text{ among } r_p\widehat{s_{k,p}} \in \widehat{l_k} \subset \widehat{H_k}\}\,.$$

We then get $\widehat{z_k}$ which, together with the argument p of the above max, provides an estimate $\widehat{C_k}$ of the source positions, for direction Π.

3.4.2 Combining information from multiple slicing directions

The above procedure is repeated for a number n_p of different slicing directions, which yields a family of $n_p \times n$ estimations of the n source positions. Matlab's algorithm `clusterdata` is again used to build n separate clusters from these $n_p \times n$ points. The final estimations $\widehat{C_k}$ of the sources are obtained as the barycenter of each cluster. As in the previous section, the distance between points is defined so as to ensure that each slicing direction contributes only once to each cluster.
Once the source positions are known, the measured potential is a linear function of the moments. These are thus estimated using a simple linear least squares minimization procedure.

4 Numerical validation

We now present numerical results obtained with `FindSources3D`, a `Matlab` code that implements the above algorithm [Bassila et al., 2008].

We simulated two data sets with `OpenMEEG`, which implements the symmetric Boundary Element Method [Gramfort et al., 2010, Kybic et al., 2005]. We considered data at the scalp level (potential measured by 128 electrodes), and also at the cortex level (potential and normal current on a 642 points mesh), in order to test the influence of the Cortical Mapping step on the quality of the source estimation. The spherical 3-layer head model is the one described in Section 2.1.

In the case of cortical data, that is with potential and current at the cortex level as computed by `OpenMEEG`, Figure 6 displays for twelve different slicing directions, the top views of the planar detected singularities. Figure 7 shows the 3D superposition of all these estimated singularities for all axis directions and the estimated source positions for all the slicing directions.

Figure 8 displays true and estimated sources from the two datasets, while Table 1 displays numerical values of the corresponding positions and moments.
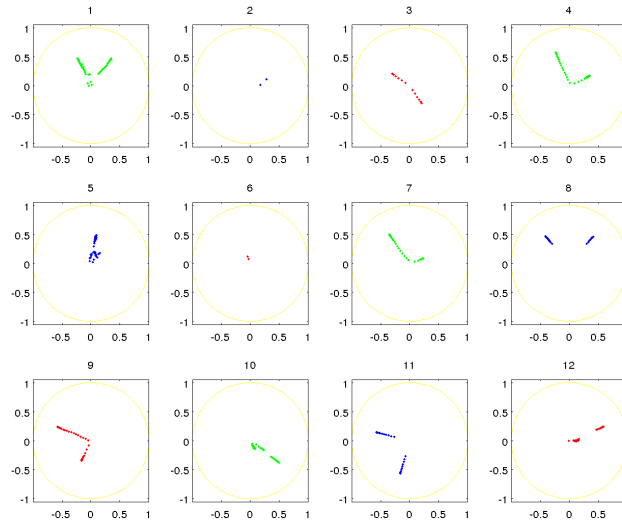

Figure 6: Top views of 2D planar singularities computed from cortical dataset for 12 different slicing directions Π.

We can see in Figures 6, 7, 8 how the present numerical results illustrate theoretical properties estabished in Section 3.3:
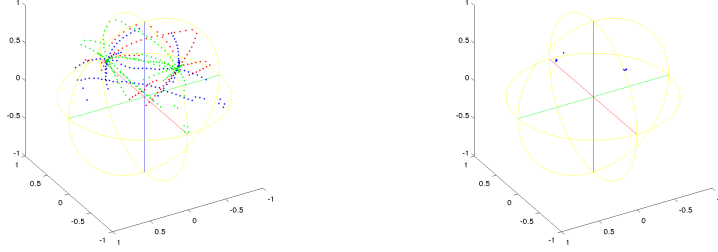
Figure 7: 3D superposition for different slicing directions: all singularities (left), estimated sources positions $\widehat{C_k}$ for all slicing directions (right).
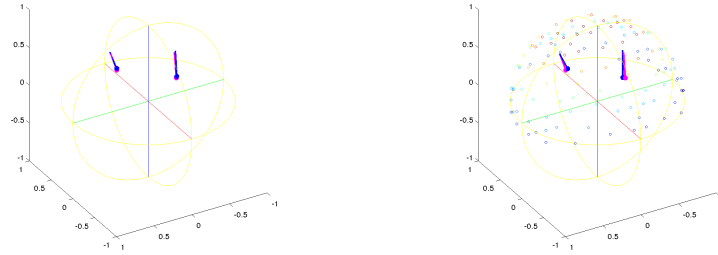

Figure 8: True *vs* estimated sources: cortical data (left), electrodes data (right).

	positions			moments		
True sources	0.2000	0.3000	0.4000	0.0000	0.2000	0.6000
	-0.3000	-0.2000	0.4000	0.1000	0.0000	0.8000
Estimated sources	0.1951	0.3056	0.4260	0.0194	0.2068	0.5874
(cortical data)	-0.3006	-0.2059	0.4208	0.0808	-0.0052	0.7993
Estimated sources	0.1917	0.2797	0.4160	0.0112	0.2579	0.5563
(electrodes data)	-0.2798	-0.1777	0.4015	0.0929	-0.0486	0.8487
Error	0.0049	-0.0056	-0.0260	-0.0194	-0.0068	0.0126
(cortical data)	0.0006	0.0059	-0.0208	0.0192	0.0052	0.0007
Error	0.0083	0.0203	-0.0160	-0.0112	-0.0579	0.0437
(electrodes data)	-0.0202	-0.0223	-0.0015	0.0071	0.0486	-0.0487

Table 1: True *vs* estimated sources from cortical and electrodes datasets.

- For a given slicing direction Π, the singularities associated with a source C_k lie in a plane H_k containing the source itself and the slicing axis (Figure 6).

- As a consequence, singularity lines associated to various slicing directions Π intersect at the sources, which allows to estimate their positions (Figure 7).

- Once these positions are estimated, the linear problem s easily solved to recover the source moments (Figure 8).

As could be expected, estimation is better when data are directly taken at the cortical level on many points. The treatment of more realistic datasets (from scalp electrodes) needs an additional Cortical Mapping step and thus achieves a less precise estimation. However the full procedure proves to be efficient enough: when estimating sources from the electrodes dataset, the global position error is less than 10% of the sphere radius (order of the cm).

5   Conclusion

We presented here some insights concerning the resolution of a source estimation problem. The techniques rely on constructive approximation, they are robust and efficient towards the EEG inverse source problem, as is illustrated by preliminary numerics.

More accuracy on source localization may be achieved by extending the present method. A first possibility would be to take into account several time samples while constraining the source positions to be fixed. Also, the computation steps concerning the singular part of the cortical potential and its 3D to 2D transformation could be made more direct, in order to limit the numerical errors.

The number of unknown sources is not yet identified automatically. However, at many steps, information is available to build good estimates of this unknown number: singular values in the rational 2D approximation scheme, residual boundary approximation error, clustering procedure, ... Work is in progress to make this number an output of the whole process, using techniques such as the Akaike information criterion to decide when increasing the number of sources is no longer significative with respect to the data.

Magnetic data from MEG (magnetoencephalography) will be incorporated as well, coupled to the available EEG, that may lead to additional precision in the source localization process.

Geometrically, the approach applies in principle to more general smooth 3D domains [Ebenfelt et al., 2001], but we did not carry out such generalizations here and only considered spherical models. One may observe that whenever the complexity of the geometry increases, so does the quantity of planar singularities associated to a source. For an ellipsoidal domain, which has been theoretically studied in [Leblond et al., 2008], we already get 2 planar singularities for each source, in each ellipse.

A Data transmission by Cortical Mapping

The Cortical Mapping Method, originally presented in [Clerc and Kybic, 2007], proceeds as follows. With the rationale of the symmetric Boundary Element method [Kybic et al., 2005], u (resp. the normal current $\sigma\partial_\nu u$) is approximated with continuous, piecewise-linear elements (resp. discontinuous, piecewise-constant elements). The discretization of these two variables on each of the boundaries $\mathbb{S}_i$, $i = 0, 1, 2$ yields a set of values which are combined in a single vector-valued variable X. The harmonic nature of u in $\Omega_1 \cup \Omega_2$, along with the fact that $\partial_\nu u = 0$ on $\mathbb{S}_2$ and the transmission conditions (2-3) are all handled by saying that X must belong to the kernel of a specific linear operator. This linear operator is represented by a dense matrix H, whose elements involve boundary integral operators. The knowledge of u on K is handled by a "measurement operator" M, such that $M X$ represents u_K, i.e. the measurements on K. Ideally one would like to find X such that $M X = u_K$ and $H X = 0$, but the ill-posedness of the Cauchy inverse problem makes it necessary to stabilise the system through a regularization. As a consequence, the method seeks X belonging to the kernel of H solving

$$\arg \min_{X \in Ker H} \|M X - u_K\|^2 + \lambda \|R X\|^2 .$$

The norms above are discrete l^2 norms, λ is a real positive Lagrange parameter to be adjusted, and R is an appropriate regularization operator. Once the minimizer X has been computed, it is immediate to extract from X the desired transmitted data u and $\sigma\partial_\nu u$ on $\mathbb{S}_0$. Results obtained by this method are illustrated in Figure 9, where the 2 sources were taken as in Section 3.1.2, and each sphere was meshed with 642 points. This figure shows the propagation of the potential measured on 128 electrodes onto the outer skull surface $\mathbb{S}_1$ and cortical surface $\mathbb{S}_0$.
Note that other transmission schemes can be obtained by best approximation with harmonic gradients, as in [Atfeh et al., 2010], and robust interpolation issues can be handled using spherical harmonics [Dautray and Lions, 2000].

B Link between 3D sources and 2D singularities

Choose a fixed slicing direction Π, as in Section 3.2. For $x \in T_p$ and $z \in T$ given by (6), let us establish equation (8) for f_p, which is equal to u_a^2 according to (7), where u_a has been defined in (5). Indeed, with $h_{k,p} = x_{3,p} - x_{3,k}$,

$$|x - C_k|^2 = (x_1 - x_{1,k})^2 + (x_2 - x_{2,k})^2 + (x_{3,p} - x_{3,k})^2 = |r_p z - z_k|^2 + h_{k,p}^2 ,$$

thus:

$$|x - C_k|^2 = (r_p z - z_k)(r_p \bar{z} - \bar{z}_k) + h_{k,p}^2 = (r_p z - z_k)\left(\frac{r_p}{z} - \bar{z}_k\right) + h_{k,p}^2$$

because $\bar{z} = 1/z$ for $z \in T$ (use that $|z|^2 = z\bar{z} = 1$). Assuming first that $z_k \neq 0$, we get

$$(r_p z - z_k)\left(\frac{r_p}{z} - \bar{z}_k\right) + h_{k,p}^2 = -\frac{r_p \bar{z}_k}{z}\left(z^2 - \frac{h_{k,p}^2 + |z_k|^2 + r_p^2}{r_p \bar{z}_k}z + \frac{z_k}{\bar{z}_k}\right) .$$

Measured potential
on scalp electrodes

Estimated potential
on scalp surface $\mathbb{S}_2$

Estimated normal current
on skull surface $\mathbb{S}_1$

Estimated potential
on skull surface $\mathbb{S}_1$

Estimated normal current
on cortical surface $\mathbb{S}_0$
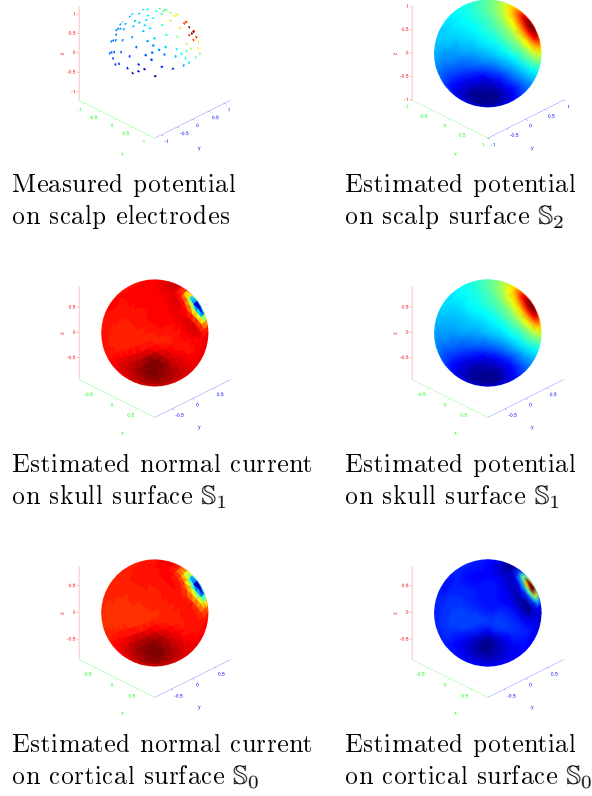
Estimated potential
on cortical surface $\mathbb{S}_0$

Figure 9: Cortical mapping reconstruction. From the potential measured on 128 electrodes (top left), the Cortical Mapping method reconstructs the normal current and the potential on all surfaces of the model. The normal current is not represented on the scalp because it is simply equal to zero in our model. Note that the spatial distribution of the potential is less sharp on the scalp and skull surfaces (top right and middle right) than on the cortex, due to the high resistivity of the skull.

Hence, for $x \in T_p$, $|x - C_k|^2$ coincides with the values on T of the function defined in the whole of $\overline{D}$ by:

$$-\frac{r_p \, \bar{z}_k}{z}(z - s_{k,p})(z - \sigma_{k,p}) \, ,$$

where the singularities $s_k = s_{k,p} \in D$ and $\sigma_k = \sigma_{k,p} \in \overline{D}$ are linked between each other and with the source parameters (C_k being determined by the quantities z_k, $h_{k,p}$ and r_p) by the relations:

$$\sigma_{k,p} \;\; = \;\; \frac{z_k}{\bar{z}_k s_{k,p}} \;\; \text{and}$$

$$s_{k,p} \;\; = \;\; \frac{z_k}{2|z_k|^2 r_p} \left(h_{k,p}^2 + r_p^2 + |z_k|^2 \sqrt{(h_{k,p}^2 + (r_p + |z_k|)^2)(h_{k,p}^2 + (r_p - |z_k|)^2)} \right) \, .$$

Also, for each slice index $p = 1, \cdots, P$,

$$|s_{k,p}| \, |\sigma_{k,p}| = 1 \text{ and } \arg s_{k,p} = \arg \sigma_{k,p} = \arg z_k \,. \tag{10}$$

With the standard convention that the square-root is positive for positive arguments (which is used throughout the paper), $s_{k,p}$ is the root with the smallest modulus and (10) ensures that $s_{k,p} \in D$ while $\sigma_{k,p} \in \overline{D}$. Recalling (7) and (5), this leads to the expression (8), or equivalently to

$$f_p(z) = \sum_{k=1}^{n} \frac{\varphi_{k,p}^2(z)}{(z - s_{k,p})^3} + 2 \sum_{\substack{k,j=1 \\ k \neq j}}^{n} \frac{\varphi_{k,p}(z)\varphi_{j,p}(z)}{(z - s_{k,p})^{3/2}(z - s_{j,p})^{3/2}} \,, \tag{11}$$

which shows that f_p admits the singularities $s_{k,p}$ in D. See below for the functions $\varphi_{k,p}$ at the numerators. The above computation exposes two useful properties of $s_{k,p}$ which are used in Section 3.4 towards the localization of C_k:

1. The argument of the complex number $s_{k,p}$ is independent of p, and equal to the argument of z_k. In any slicing direction that separates the sources (that is if $z_k \neq z_j$ for $k \neq j$, which generically holds), this property allows:

   - to determine the number of sources n, since the quantity of sources should be equal to the number of values taken by the complex argument of $s_{k,p}$, as k and p vary;

   - for any fixed index k_0, to track $s_{k_0,p}$ among all the $s_{k,p}$ in any slice p (the complex argument of $s_{k_0,p}$ does not depend on p);

   - to determine the argument of z_{k_0}.

2. When p varies (for $x_{3,p} \in (-1, 1)$), the modulus of $r_p \, s_{k,p}$ increases monotonically for $x_{3,p} < x_{3,k}$ (decreases monotonically for $x_{3,k} < x_{3,p}$), and attains a maximum when $x_{3,k} = x_{3,p}$ or $h_{k_0,p} = 0$, in which case one has $r_p \, |s_{k_0,p}| = |z_{k_0}|$. This second property allows us to determine $|z_{k_0}|$, whence finally z_{k_0}.

Also, if we put $p_k = (p_{1,k}, p_{2,k}, p_{3,k})$ for the moments and $\varrho_k = p_{1,k} + ip_{2,k}$, we get from (5) that:

$$\varphi_{k,p}(z) = \frac{1}{8\pi} \frac{\bar{\varrho}_k}{(r_p \bar{z}_k)^{3/2}} \frac{\sqrt{z}}{(\sigma_{k,p} - z)^{3/2}} \, \pi_{2,k,p}(z)$$

are uniformly bounded in D and $\pi_{2,k,p}$ are polynomials of degree 2 (see also [Baratchart et al., 2006]):

$$\pi_{2,k,p}(z) = r_p z^2 + 2 \frac{p_{3,k} h_{k,p} - \mathrm{Re} \, (z_k \bar{\varrho}_k)}{\bar{\varrho}_k} z + \frac{\varrho_k}{\bar{\varrho}_k} \, r_p \,.$$

Finally, whenever $z_k = 0$ (that is when the associated C_k lies on the vertical axis), then $|x - C_k|^2 = r_p^2 + h_{k,p}^2$ is a constant and the corresponding term of (8) becomes a rational function of z which assumes the form $\pi_{2,k,p}(z)/z$ for the above mentioned polynomials $\pi_{2,k,p}$. In this situation, the function f_p to be approximated has a unique (double) pole in D at 0, in every planar section p, which will be revealed by the Rational Approximation step. The sum of the

roots of the polynomial $\pi_{2,k,p}$ is equal to $-\frac{2p_{3,k}}{\bar{\varrho}_k\, r_p} h_{k,p}$. If $p_{3,k} \neq 0$, the behaviour of these roots still allows to compute the index p such that $h_{k,p} = 0$, and to finally locate the singularity C_k. The situation where $z_k = 0$ and $p_{3,k} = 0$ however is degenerated w.r.t. the present choice of Π, which is the reason why several slicing directions should be used.

C Best Rational Approximation Schemes

C.1 Best Rational Approximation

From the knowledge of f_p on the surrounding circle T, the $s_{k,p}$ in D, $k = 1, ..., n$ are localized using Rational Approximation on T, with poles in D. Indeed, as we will see, the poles $s^*_{k,p}$ of such approximants accumulate to the singularities $s_{k,p}$ of the approximated function f_p.

Let us first briefly explain the best quadratic Rational Approximation techniques that are used.

As explained in Section 3.3, the singularities $s_{k,p}$ can be described both as branchpoints and as triple poles of f_p. For a single source, we noted that f_p is exactly a degree 3 rational function and the singularity $s_{k,p}$ is itself a triple pole. For multiple sources, the situation is not so simple, but the property that poles lines pass near the singularities still remains. This makes it interesting to consider two Rational Approximation schemes: one with simple poles and the other with triple poles.

We define $\mathcal{R}_m$ to be the set of rational functions R_m with less than m poles in D: $R_m = \dfrac{\pi_m}{q_m}$, where π_m and q_m are polynomials such that deg $\pi_m <$ deg $q_m \leq m$, and where the zeroes of q_m belong to D.

A best quadratic rational approximant to f_p in $\mathcal{R}_m$ is a function $R^*_m \in \mathcal{R}_m$, verifying:

$$\|f_p - R^*_m\| = \min_{R_m \in \mathcal{R}_m} \|f_p - R_m\| \,, \tag{12}$$

for the $L^2(T)$ norm, see [Baratchart et al., 1992]. Existence and non-uniqueness of R^*_m are discussed in [Baratchart et al., 1992]. Concerning constructive aspects, efficient algorithms to generate local minima are obtained using Schur parametrization [Marmorat et al., 2002]. Computation of R^*_m is made effective through suitable parametrization of rational functions, using gradient algorithms [Marmorat et al., 2002].

Generally and properly speaking, for functions $f_p \in L^2(T)$, the approximation class $\mathcal{R}_m$ should be the set of "meromorphic" functions with less than m poles in D. Such a meromorphic function is the sum of a rational function $\frac{\pi_m}{q_m}$ and of a function h "holomorphic" (or equivalently "analytic") in D (which has no singularities in D but may have poles outside D). Because

$$\frac{\pi_m}{q_m} + h = \frac{\pi_m + hq_m}{q_m} \,,$$

we see that a meromorphic function coincides with the quotient of a holomorphic function by a polynomial.

Further, whenever f_p has singularities only in D and is analytic in $\mathbb{C} \setminus \overline{D}$ (and vanishes at ∞), its best meromorphic approximant coincides with its best rational approximant with poles in D. This is the reason why we explain in C.2 how

to get, in general, this part of f_p, analytic in $\mathbb{C} \setminus \overline{D}$, which shares the singularities of f_p in D but as no singularity outside D.

C.2 2D Analytic Projection

Observe from B that f_p possesses singularities both inside and outside the unit disk, that are linked to each other and to the sources C_k, see e.g. (10).
Indeed, the representation (8) involves the singularities $s_{k,p}$ of f_p in D but also the additional reflected ones $\sigma_{k,p}$ (hidden in $\varphi_{k,p}$) outside D. First, these are linked with each other by (10). Next, the Rational Approximation algorithms available for data on T require the singularities of the approximated functions to belong to a region of the plane limited by T (see Section 3.3; in particular, this leads to a lower degree of the approximants, that also possess strong robustness properties). We thus choose to keep only those of the singularities $s_{k,p}$ of f_p that belong to the disk D, and we need to filter the $\sigma_{k,p}$ out.
It is easily seen from (8) that the function f_p is continuous on T, because none of its singularities belong to T. Thus it belongs to the Lebesgue space $L^2(T)$ of functions with square summable modulus on T. Consequently, it can be uniquely written on T as the sum $f_p = F + F_o$, where F is the holomorphic projection of f_p in $\mathbb{C} \setminus \overline{D}$ and vanishes at ∞, while F_o is holomorphic in D. Actually, F and F_o respectively belong to the Hardy classes of $\mathbb{C} \setminus \overline{D}$ and of D, their traces on T belonging to $L^2(T)$ [Rudin, 1987]. The Hardy-Hilbert spaces H_-^2, resp. H_+^2 are the sets of functions analytic in $\mathbb{C} \setminus \overline{D}$ (vanishing at ∞), resp. analytic in D, and bounded in $L^2(T)$ norm (i.e. the space of $L^2(T)$ functions with vanishing Fourier coefficients of positive indices, resp. of strictly negative indices). We can directly compute F from the Fourier series expansion of f_p on T:

$$f_p(e^{i\theta}) = \sum_{l \in \mathbb{Z}} F_l \, e^{il\theta} \,, \quad \sum_{l \in \mathbb{Z}} |F_l|^2 < \infty$$

$$\Rightarrow F(z) = (P_- f_p)(z) = \sum_{l<0} F_l \, z^l \,, \ |z| \geq 1 \,, \tag{13}$$

if P_- denotes the orthogonal "anti-analytic" projection from $L^2(T)$ onto H_-^2. The important point here is that f_p and F share the same singularities inside D while F has no singularities outside D, since F possesses an expression analogous to (8), with identical denominators, but numerators given by smooth functions. This is necessary for the best Rational Approximation problem o be solved among rational (no longer meromorphic) functions with poles in D.
We shall then assume from now on, and already for the computations of Section 3.3, that f_p is analytic in $\mathbb{C} \setminus \overline{D}$, and vanishes at ∞, without loss of generality.

C.3 Behaviour of Simple Poles with respect to Singularities and Sources

If the degree m is not preliminarily given, observe that its estimation can be obtained by computing the boundary error on T (the value of the criterion in (12)) for increasing values of m, until it is small enough, see Remark 1. This will happen in principle for $m \simeq 3n$, the number of singularities of f_p in D according to their multiplicity.

For such a value of m, compute the best approximant R_m^* itself (that the approximant should be computed only once, for m large enough for the error to be sufficiently small, is one of the features that make this scheme efficient).

In sections p close to C_k, f_p is (numerically) close to a rational function with poles at $(s_{k,p})$. Thus, for m large enough, typically $m \geq 3n$, the m poles of R_m^* must then be located near the $(s_{k,p})$ (see Property (P), C.5), and they should be packed in a number of clusters coinciding with the number n of sources.

This is illustrated in Figures 10–12 where $m = 1, 2$ and 3 simple poles cases are respectively shown for the same situation with $n = 2$ sources as in Section 3.1.2. For $k = 1, 2$ and varying p, theoretically known singularities $(r_p \, s_{k,p})$ are shown in disks D_p as green dots whereas estimated poles are shown with red dots. Black dots represent the sources C_1, C_2.
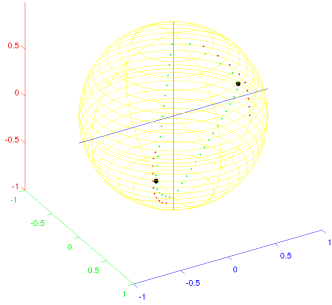
Figure 10: 1 simple pole
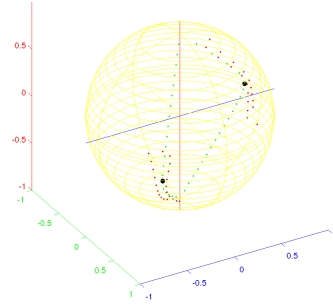
Figure 11: 2 simple poles
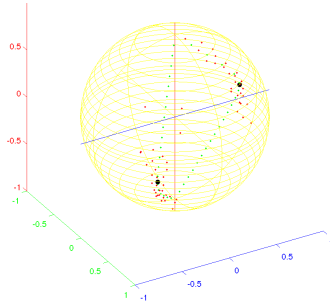
Figure 12: 3 simple poles

C.4 Behaviour of Triple Poles with respect to Singularities and Sources

Recall that the singularities $s_{k,p}$ that we aim at recovering appear at *triple* poles of f_p, from (8), which motivates the computation of best rational approximants with *triple* poles.

Recall that for a single source ($n = 1$), then (8) is to the effect that f_p is a rational function with a triple pole in D, see (9). Hence, its best rational approximant with a single triple pole in D should coincide with f_p itself. Whenever $n > 1$, the situation is of course more complicated since f_p admits the $s_{k,p}$ both as triple poles and branchpoints. However, as we shall see, the behavior of poles dominates whence its best rational approximant with triple poles still allows to recover the $s_{k,p}$.

These best rational approximants with triple poles in D are functions $R_{3m}^* = \pi_{3m}/q_m^3 \in \mathcal{R}_{3m}$ that satisfy (12), where π and q are polynomials such that $\deg q_m \leq m$, $\deg \pi_{3m} < 3m$. An advantage is that the computations can then be performed with a lower degree than in the simple poles case, since $m = n$ is enough.

Again, even though f_p is not a rational function (it admits poles *and branchpoints located at the same place*), it is (numerically) close to rationals of $\mathcal{R}_3$ with *a single triple pole* ($m = 1$), in plane sections p close to the one containing (C_k), even for several sources, when $n > 1$.

For such data f_p, close to a rational function of $\mathcal{R}_3$ with a single triple pole, say t, in D, then the single triple pole of the best rational approximant is close to t, see the robustness property (P'), C.6.

Hence the above best approximants R_{3m}^* possess an even stronger property: in general a single ($m = 1$) triple pole is enough in order to localize several singularities $s_{k,p}$ in D, hence several sources (C_k) ($n \geq 1$), by varying p. Indeed, in the slice p containing a source C_k, the single triple pole s_p^* of R_3^* is close to the associated singularity $s_{k,p}$.

This situation is illustrated in Figure 13 for the same source configuration as the one used for Figures 10–12. As previously, sources are indicated with black dots, green dots show the known theoretical positions of singularities while red dots show the triple poles. One can notice that there is only one pole trajectory for both singularity lines. Thus the triple pole line does not follow the singularity lines as in the single pole case. However, close to sources, the triple poles approximate the singularity lines quite well.
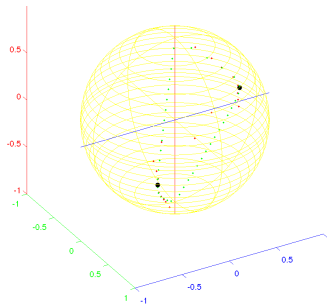

Figure 13: 1 triple pole

C.5 Behaviour of Simple Poles of Rational Approximants

We give a few additional considerations concerning the asymptotic behaviour of the poles.

In situations where f_p is already a rational function R_N of $\mathcal{R}_N$, then its best rational approximant R_m^* coincides with f_p for $m \geq N$. This result is robust in the sense of property (P) below. Observe that whenever $n \geq 2$, the function f_p has poles *and* branchpoints in D, and it can be shown that the degree of the denominator q_m of R_m^* is in fact equal to m, for each integer m. Property (P) can be deduced from [Baratchart, 1986, Prop. 5]:

(P) *Whenever f_p is close (in $L^2(T)$) to a rational function R_N, then the poles of R_m^* accumulate to those of R_N, as m increases.*

Further, deep convergence results from potential theory [Baratchart and Yattselev, 2009] assert that, for a function f_p as in the present situation (which admits finitely many poles and branchpoints in D and has a smooth behaviour near T), the m poles of R_m^* converge (in some weak sense) to the singularities $(s_k) = (s_{k,p})$ of f_p as m increases (where, for notational simplicity, the index p is fixed and has been omitted).

For $n = 2$, the sequence of counting probability measures of the poles of R_m^* will asymptotically charge s_1 and s_2 (the poles will accumulate "near" s_1 and s_2), while only finitely many poles stay away from s_1, s_2 and from the arc of circle orthogonal to T joining them [Baratchart et al., 2001].

These results are related to the fact that, for $n = 2$, f_p can be represented as:

$$ f_p(z) = R_6(z) + R_2(z) \int_{s_1}^{s_2} \frac{dt}{(z-t)\sqrt{(t-s_1)(s_2-t)}} \, , $$

for rationals $R_2 \in \mathcal{R}_2$ and $R_6 \in \mathcal{R}_6$ with, respectively, two simple poles for R_2 and two triple poles for R_6, at s_1 and s_2. This result is used in [Baratchart and Yattselev, 2009] to study the behaviour of the poles of best rational approximants.

C.6 Behaviour of Triple Poles of Rational Approximants

We have the robustness property:

(P') *For a function f_p, close to a rational of $\mathcal{R}_3$ with a single triple pole $t \in D$, then the triple pole t^* of its best rational approximant R_3^* (with a single triple pole in D) and t are close to each other.*

Property (P') is a restatement of:

Proposition 1 *Let $R_3(z) = \pi(z)/(z-t)^3$ be a rational function of $\mathcal{R}_3$ with a triple pole $t \in D$, strictly proper ($\deg \pi < 3$), and irreducible ($\pi(s) \neq 0$). Then, there exists $K > 0$ such that for all rational function $\tilde{R}_3(z) = \tilde{\pi}(z)/(z-b)^3$ with a triple pole $b \in D$, the following inequality holds: $|t - b| \leq K\|R_3 - \tilde{R}_3\|$, for the $L^2(T)$ norm.*

Indeed, as a corollary, if $\|f_p - R_3\| \leq \epsilon$ (in $L^2(T)$ norm), for some $\epsilon > 0$ and $R_3 \in \mathcal{R}_3$ with a single triple pole t in D, then we have the inequality: $|t - t^*| < K\epsilon$.

Proof of Proposition 1: Let $R = \pi/q$, and $\tilde{R} = \tilde{\pi}/\tilde{q}$, be two proper rational (irreducible) functions in $L^2(T)$: in particular, $\pi, q, \tilde{\pi}, \tilde{q}$ are polynomials, and

the roots of q and $\tilde{q}$ lie inside the open unit disk D (q and $\tilde{q}$ are called "stable" polynomials).

<u>Step 1</u> We look for a lower bound to

$$d(R, \tilde{R}) \;=\; \left\| \frac{\pi}{q} \;-\; \frac{\tilde{\pi}}{\tilde{q}} \right\|$$

($L^2(T)$ norm). If n is the degree of $\tilde{q}$, put $\check{\tilde{q}}(z) = z^n \overline{\tilde{q}(1/\bar{z})}$ for its reciprocal polynomial. Then $\tilde{q}/\check{\tilde{q}}$ has modulus 1 on the unit circle, and we also have:

$$d(R, \tilde{R}) \;=\; \left\| \frac{\pi}{q} \frac{\tilde{q}}{\check{\tilde{q}}} \;-\; \frac{\tilde{\pi}}{\check{\tilde{q}}} \right\| .$$

From the orthogonal decomposition of $L^2(T)$ into Hardy spaces of analytic functions [Rudin, 1987], and because $P_-(\tilde{\pi}/\check{\tilde{q}}) = 0$, since the poles of $\tilde{\pi}/\check{\tilde{q}}$ belong to $\mathbb{C} \setminus \overline{D}$.
we get that:

$$d(R, \tilde{R}) \;\geq\; \left\| P_- \left(\frac{\pi}{q} \frac{\tilde{q}}{\check{\tilde{q}}} \right) \right\| . \tag{14}$$

Remark 2 The right hand-side of (14) vanishes if and only if q is a divisor of $\tilde{q}$.

<u>Step 2</u> In the particular case where $R \in \mathcal{R}_3$ and $\tilde{R}$ have a single triple pole respectively at $t \in D$, and and at $b \in D$, then $q(z) = (z - t)^3$, $\tilde{q}(z) = (z - b)^3$, $\check{\tilde{q}}(z) = (1 - \bar{b}z)^3$, and we can evaluate this right hand-side by a fractional decomposition. Indeed, expand $\pi(z)\tilde{q}(z)$ in powers of $(z - t)$ in order to obtain:

$$P_- \left(\frac{\pi}{q} \frac{\tilde{q}}{\check{\tilde{q}}} \right) \;=\; P_- \left(\frac{1}{(1 - \bar{b}z)^3} \left(\frac{A_1}{z - t} \;+\; \frac{A_2}{(z - t)^2} \;+\; \frac{A_3}{(z - t)^3} \right) \right) \tag{15}$$

with

$$\begin{aligned} A_1 &= 3\pi(s)(t - b) + 3\pi'(t)(t - b)^2 + \pi''(t)(t - b)^3/2 \,, \\ A_2 &= 3\pi(s)(t - b)^2 + \pi'(t)(t - b)^3 \,, \quad A_3 = \pi(t)(t - b)^3 \,. \end{aligned}$$

Expanding now $1/\check{\tilde{q}}$ in a neighbourhood of $z = t$ in D, we get:

$$\frac{1}{\check{\tilde{q}}(z)} \;=\; \frac{1}{(1 - \bar{b}z)^3} \;=\; \frac{1}{(1 - \bar{b}s)^3} \left(1 \;+\; \frac{3\bar{b}(z - t)}{1 - \bar{b}t} \;+\; \frac{6\bar{b}^2(z - t)^2}{(1 - \bar{b}t)^2} \right) + O((z-t)^3) \,.$$

The P_- projections in (15) can then be expressed as:

$$\begin{aligned} P_- \left(\frac{1}{(1 - \bar{b}z)^3} \frac{1}{z - t} \right) &= \tfrac{\alpha}{z-s} \,, \\ P_- \left(\frac{1}{(1 - \bar{b}z)^3} \frac{1}{(z - t)^2} \right) &= \tfrac{\alpha}{(z-t)^2} + \tfrac{\beta}{z-t} \,, \\ P_- \left(\frac{1}{(1 - \bar{b}z)^3} \frac{1}{(z - t)^3} \right) &= \tfrac{\alpha}{(z-t)^3} + \tfrac{\beta}{(z-t)^2} + \tfrac{\gamma}{z-t} \,, \end{aligned}$$

where

$$\alpha \;=\; \frac{1}{(1 - \bar{b}t)^3} \,, \quad \beta \;=\; \frac{3\bar{b}}{(1 - \bar{b}t)^4} \,, \quad \gamma \;=\; \frac{6\bar{b}^2}{(1 - \bar{b}t)^5} \,.$$

Thus:
$$P_- \left(\frac{\pi}{q} \frac{\tilde{q}}{\check{\tilde{q}}} \right) \; = \; \Phi_{t,b}(z) \; = \; (t-b)\frac{N_{t,b}(z)}{(z-t)^3} \; = \; (t-b)\Psi_{t,b}(z)\,,$$

where $\Phi_{t,b}$, $\Psi_{t,b}$ are rational functions, and $N_{t,b}$ is a polynomial of degree 2, as follows from:
$$\Phi_{t,b}(z) = \frac{\alpha A_3}{(z-t)^3} + \frac{\alpha A_2 + \beta A_3}{(z-t)^2} + \frac{\alpha A_1 + \beta A_2 + \gamma A_3}{z-t}\,.$$

Using (14), we thus get:
$$d(R, \tilde{R}) \; \geq \; \|\Phi_{t,b}\|\,.$$

Note that $\Phi_{t,b}$, $\Psi_{t,b}$, and $N_{t,b}$ have continuous coefficients in the variable $b \in D$. In particular, for $b = t \in D$:
$$\Phi_{t,t}(z) = 0\,, \qquad \Psi_{t,t}(z) = \frac{3\tilde{\pi}(t)}{(1-|t|^2)^3}\frac{1}{z-t}\,.$$

<u>Step 3</u> Consider the $L^2(T)$ norms of $\Phi_{t,b}$ and $\Psi_{t,b}$ as functions of b, and put
$$\phi(b) = \|\Phi_{t,b}\|\,, \; \psi(b) = \|\Psi_{t,b}\|\,, \text{ whence } \phi(b) = |t-b|\psi(b)\,.$$

From (14), we now have that
$$d(R, \tilde{R}) \; \geq \; \phi(b)\,.$$

The above expressions are then to the effect that ϕ and ψ are continuous functions of $b \in D$. Further, ϕ and ψ admit continuous extensions up to the closed disk $\overline{D}$, and ψ does not vanish on $\overline{D}$. Indeed, let $|b| = 1$ and $b_n \in D$, $b_n \to b$. Then, $\forall z \in D$, $\tilde{q}_n(z)/\check{\tilde{q}}_n(z) = (z-b_n)^3/(1-\bar{b}_n z)^3$ converges to the constant $-b^3$, whence $(\pi\tilde{q}_n)/(q\check{\tilde{q}}_n) \to -b^3\tilde{\pi}/\tilde{q}$ in $L^2(T)$. Since $P_-(\pi/q) = \pi/q = R$ (because $\mathcal{R}_m$ is contained in the above mentioned Hardy class of functions analytic in $\mathbb{C} \setminus \overline{D}$ and by definition), we deduce that ϕ continuously extends to T and that $\phi(b) = \|R\|, \quad \forall b \in T$. Hence, ψ also admits a continuous extension on T and $\psi(b) = \|R\|/|t-b|, \; \forall b \in T$.

<u>Step 4</u> Finally, the continuous positive function ψ attains its minimal value $K' \geq 0$ in $\overline{D}$ at some point $b_0 \in \overline{D}$. In order to establish by contradiction that $K' > 0$, assume that $K' = 0$; then $\psi(b_0) = 0$ which implies $\phi(b_0) = 0$. Then $b_0 \notin T$, since $\phi_{|_T} = \|R\|$. But if $b_0 \in D$, then necessarily $b_0 = t$, the unique point in D where ϕ vanishes, from Remark 2. However, because $\left\|\frac{1}{z-t}\right\| = (1-|t|^2)^{-\frac{1}{2}}$, we have $\psi(t) = 3|\tilde{\pi}(t)|(1-|t|^2)^{-\frac{7}{2}}$. Because $R = \pi/q$ is irreducible, then $\pi(t) \neq 0$, so $\psi(t) \neq 0$, and this is a contradiction. Hence, $K' > 0$.

<u>Step 5</u> Thus $\psi(b) \geq K' > 0$ whence, with $K = 1/K'$, $\phi(b) \geq |t-b|$ and:
$$|t-b| \; \leq \; K\phi(b) \; \leq \; Kd(R, \tilde{R})\,,$$

which achieves the proof of Proposition 1, with $R_3 = R$. $\qquad\qquad\square$

Remark 3 The expressions of α, β, γ lead to a similar result for the hyperbolic distance:
$$\exists K_0 > 0, \quad \left| \frac{t-b}{1-\bar{b}t} \right| \; \leq \; K_0\phi(b) \; \leq \; K_0 d(R, \tilde{R})\,.$$

References

A. Ben Abda, F. Ben Hassen, J. Leblond, and M. Mahjoub. Sources recovery from boundary data: a model related to electroencephalography. Math. and Comput. Modelling, 49:2213–2223, 2009.

G. Alessandrini, L. Rondi, E. Rosset, and S. Vessella. The stability for the cauchy problem for elliptic equations. Inverse Problems, 25:123004 (47pp), 2009.

B. Atfeh, L. Baratchart, J. Leblond, and J.R. Partington. Bounded extremal and Cauchy-Laplace problems on the sphere and shell. J. on Fourier Analysis and Applications, 16:177–203, 2010.

A. El Badia. Inverse source problem in an anisotropic medium by boundary measurements. Inverse Problems, 21:1487–1506, 2005.

A. El Badia and T. Ha-Duong. An inverse source problem in potential analysis. Inverse Problems, 16:651–663, 2000.

L. Baratchart. Existence and generic properties for L^2 approximants of linear systems. I.M.A. Journal of Math. Control and Identification, 3:89–101, 1986.

L. Baratchart and M. Yattselev. Meromorphic approximants to complex Cauchy transforms with polar singularities. Mat. Sb., 200:3–40, 2009.

L. Baratchart, M. Olivi, and F. Wielonsky. On a rational approximation problem in the real Hardy space H_2. Theoretical Computer Science, 94:175–197, 1992.

L. Baratchart, H. Stahl, and F. Wielonsky. Asymptotic uniqueness of best rational approximants of given degree to Markov functions in L^2 of the circle. Constructive Approximation, 17:103–138, 2001.

L. Baratchart, A. Ben Abda, F. Ben Hassen, and J. Leblond. Recovery of point-wise sources or small inclusions in 2D domains and rational approximation. Inverse Problems, 21:51–74, 2005.

L. Baratchart, J. Leblond, and J.-P. Marmorat. Inverse source problem in a 3D ball from best meromorphic approximation on 2D slices. Electronic Trans. in Numerical Analysis, 25:41–53, 2006.

R. Bassila, M. Clerc, J. Leblond, J.-P. Marmorat, and T. Papadopoulo. Find-sources3d, 2008. URL http://www-sop.inria.fr/apics/FindSources3D/. Software.

C.-G. Bénar, R.N. Gunn, C. Grova, B. Champagne, and J. Gotman. Statistical maps for EEG dipolar source localization. IEEE Trans. on Biomedical Engineering, 52(3):401–413, 2005.

M. Clerc and J. Kybic. Cortical mapping by laplace-cauchy transmission using a boundary element method. Inverse Problems, 23:2589–2601, 2007.

B. Cuffin. A method for localizing EEG sources in realistic head models. IEEE Trans. on Biomedical Engineering, 42:68–71, 1995.

R. Dautray and J.-L. Lions. Mathematical Analysis and Numerical Methods for Science and Technology, volume 2. Springer, 2000.

P. Ebenfelt, D. Khavinson, and H.S. Shapiro. An inverse problem for the double layer potential. Computational Methods and Function Theory, 1:387–402, 2001.

A. Gramfort, T. Papadopoulo, E. Olivi, and M. Clerc. OpenMEEG: opensource software for quasistatic bioelectromagnetics. BioMedical Engineering OnLine, 9(45), September 2010. URL http://hal.inria.fr/inria-00523624.

V. Isakov. Inverse problems for partial differential equations, volume 127 of Applied Mathematical Sciences. Springer, 1998.

D. Kandaswamy, T. Blu, and D. Van De Ville. Analytic sensing: Noniterative retrieval of point sources from boundary measurements. SIAM J. on Scientific Computing, 31:3179–319, 2009.

V.A. Kozlov, V.G. Mazya, and A.V. Fomin. An iterative method for solving the Cauchy problem for elliptic equations. Comput. Maths. Math. Phys., 31 (1):45–52, 1992.

J. Kybic, M. Clerc, T. Abboud, O. Faugeras, R. Keriven, and T. Papadopoulo. A common formalism for the integral formulations of the forward EEG problem. IEEE Trans. on Medical Imaging, 24:12–28, 2005.

J. Leblond, C. Paduret, S. Rigat, and M. Zghal. Source localisation in ellipsoids by best meromorphic approximation in planar sections. Inverse Problems, 24: 035017, 2008.

J.-P. Marmorat and M. Olivi. Rational approximation: RARL2, 2004. URL http://www-sop.inria.fr/apics/RARL2/rarl2-eng.html. Software.

J.-P. Marmorat, M. Olivi, B. Hanzon, and R.L.M. Peeters. Matrix rational H^2 approximation: a stage-space approach using Schur parameters. In Proceedings of CDC'02, Las Vegas, 2002.

J. C. Mosher, P.S. Lewis, and R.M. Leahy. Multiple dipole modeling and localization from spatio-temporal meg data. IEEE Trans. on Biomedical Engineering, 39(6):541–553, 1992.

K.D. Phung. Remarques sur l'observabilité pour l'équation de laplace. ESAIM: COCV, 9:621–635, 2003.

W. Rudin. Real and Complex Analysis. McGraw-Hill, 1987.

M. Scherg, T. Bast, and P. Berg. Multiple source analysis of interictal spikes: goals, requirements, clinical value. J. of Clinical Neurophysiology, 16:214–238, 1999.

B.D. Van Veen and K.M. Buckley. Beamforming: a versatile approach to spatial filtering. IEEE Acoustics, Speech, Signal Processing Mag., 5:4–24, April 1988.

S. Vessella. Locations and strengths of point sources: stability estimates. Inverse Problems, 8:911–917, 1992.

M. Zghal. Problèmes inverses pour l'équation de Laplace en dimension 3, application à l'éléctroencéphalographie. PhD thesis, ENIT, Univ. Tunis El Manar, 2010.

Contents